العدد 19A1 كانون الاول 2025
No.19A Dec. 2025
المجلة العراقية للبحوث الإنسانية والإجتماعية والعلمية
Iraqi Journal of Humanitarian, Social and Scientific Research
Print ISSN 2710-0952 Electronic ISSN 2790-1254

Evaluating the Therapeutic Impact of Drug-Loaded Nanoparticles on Apoptotic Pathways in Cancer Cells

Abdulah Abd Ulkarem Abdulah Ismail, balmaystrw204@gmail.com

1. Abstract:

Background: Quercetin exhibits potent anticancer activity but suffers from poor bioavailability, limiting its clinical translation. Nanoparticle-based delivery offers a promising solution, yet mechanistic validation often remains superficial, lacking transcriptional-level evidence linking nanoformulation to apoptotic commitment.

Methods: Quercetin-loaded PLGA nanoparticles (QNPs) were synthesized via single-emulsion solvent evaporation and characterized (DLS, TEM, UV-Vis). In MCF-7 breast cancer cells, we employed a multi-layered experimental platform: cytotoxicity (MTT), apoptosis quantification (Annexin V/PI flow cytometry), caspase activation (luminescent assays), ROS detection (DCFH-DA), and critically RT-qPCR profiling of eight apoptosis-related genes (*BAX*, *BCL-2*, *CASP3/9*, *TP53*, *PUMA*, *FAS*, *TNFRSF10B*), compliant with MIQE guidelines. Empty NPs (ENPs) and free quercetin (FQ) served as controls.

Results: QNPs (size: 142.3 ± 8.7 nm; EE%: 87.4 ± 3.1%) reduced IC_{50} by 47% versus FQ (22.1 ± 1.8 µM vs. 41.7 ± 2.6 µM; $p < 0.001$) and induced 3.2-fold higher apoptosis. Caspase-3/7 and caspase-9 activities increased 4.1- and 3.8-fold, respectively. RT-qPCR revealed a coordinated intrinsic apoptotic signature: *BAX* ↑ 3.82-fold, *BCL-2* ↓ to 0.28-fold (→ *BAX/BCL-2* ratio ↑ 13.6×), *CASP9* ↑ 4.15-fold, and *TP53* ↑ 2.94-fold ($p < 0.01$–0.001), while extrinsic markers (*FAS*, *TNFRSF10B*) were unchanged ($p > 0.05$). The *BAX/BCL-2* ratio strongly correlated with apoptosis ($r = 0.93$, $p < 0.001$).

Conclusion: QNPs overcome quercetin's bioavailability barrier to drive p53-mediated mitochondrial apoptosis via transcriptional reprogramming. RT-qPCR provides indispensable genomic insight, establishing *BAX/BCL-2* dysregulation as a central, predictive node. This integrated approach sets a reproducible benchmark for mechanistic validation in nanomedicine.

2. Keywords :PLGA nanoparticles, quercetin, MCF-7, apoptosis, RT-qPCR, caspase-3/9, *BAX/BCL-2* ratio, intrinsic pathway, nanomedicine, molecular validation

تقييم الأثر العلاجي للجسيمات النانوية المحملة بالأدوية على مسارات الاستماتة في الخلايا السرطانية

عبد الله عبد الكريم عبد الله إسماعيل

balmaystrw204@gmail.com

1.الملخص:

الخلفية: يُظهر الكيرسيتين فعالية قوية مضادة للسرطان، ولكنه يعاني من انخفاض التوافر الحيوي، مما يحد من استخدامه السريري. يوفر توصيل الأدوية باستخدام الجسيمات النانوية حلاً واعداً، إلا أن التحقق من الآلية غالباً ما يظل سطحياً، ويفتقر إلى أدلة على مستوى النسخ تربط التركيبة النانوية بالالتزام بالاستماتة. الطرق: تم تصنيع جسيمات نانوية من البوليمر PLGA محملة بالكيرسيتين (QNPs) عن طريق تبخير المذيب في مستحلب أحادي، وتم توصيفها) باستخدام تقنيات DLS و TEMو .(UV-Visفي خلايا سرطان الثدي MCF-7 ، استخدمنا منصة تجريبية متعددة الطبقات: السمية الخلوية(MTT) ، والقياس الكمي للاستماتة) قياس التدفق الخلوي (Annexin V/PI، وتنشيط الكاسبيز (الفحوصات المضيئة)، والكشف عن أنواع الأكسجين التفاعلية(DCFH-DA) ، والأهم من ذلك، تحديد خصائص RT-qPCR لثمانية جينات مرتبطة بالاستماتة(BAX ، BCL-2، CASP3/9، TP53، PUMA، FAS، TNFRSF10B)، بما يتوافق مع إرشادات MIQE. استُخدمت الجسيمات النانوية الفارغة (ENPs) والكيرسيتين الحر (FQ)كعناصر تحكم. النتائج: قللت الجسيمات النانوية الفارغة (QNPs) (الحجم: 142.3 ± 8.7 نانومتر؛ نسبة التغليف: 87.4 ± 3.1%) تركيز التثبيط النصفي (IC_{50}) بنسبة 47% مقارنةً بالكيرسيتين الحر (22.1 ± 1.8 ميكرومتر مقابل 41.7 ± 2.6 ميكرومتر؛ $p < 0.001$ ، وحفزت موت الخلايا المبرمج بمقدار 3.2 ضعف. كما زاد نشاط كاسبيز-7/3 وكاسبيز-9 بمقدار 4.1 و3.8 ضعف على التوالي. كشف تحليل RT-qPCR عن بصمة داخلية متناسقة للاستماتة الخلوية: ارتفاع BAX بمقدار 3.82 ضعف، وانخفاض BCL-2 بمقدار 0.28 ضعف) مما أدى إلى زيادة نسبة BAX/BCL-2 بمقدار 13.6 ضعف(، وارتفاع CASP9 بمقدار 4.15 ضعف، وارتفاع TP53 بمقدار 2.94 ضعف($p < 0.01–0.001$) ، بينما لم تتغير المؤشرات الخارجية (FAS، TNFRSF10B) ($p > 0.05$). وارتبطت نسبة BAX/BCL-2 ارتباطًا وثيقًا بالاستماتة الخلوية($r = 0.93$ ، $p < 0.001$).

الخلاصة: تتغلب جسيمات الكيرسيتين النانوية (QNPs) على عائق التوافر الحيوي للكيرسيتين لتحفيز الاستماتة الخلوية الميتوكوندرية بوساطة p53 عبر إعادة برمجة النسخ الجيني. يُوفّر تفاعل البوليميراز المتسلسل الكمي في الوقت الحقيقي (RT-qPCR) رؤى جينومية لا غنى عنها، مُثبتًا أن خلل تنظيم BAX/BCL-2 يُمثّل عقدة تنبؤية مركزية. يُرسي هذا النهج المتكامل معيارًا قابلًا للتكرار للتحقق من الآليات في الطب النانوي.

2.الكلمات المفتاحية: جسيمات نانوية منPLGA ، كيرسيتين، MCF-7، موت الخلايا المبرمج، RT-qPCR، كاسبيز-9/3، نسبةBAX/BCL-2 ، المسار الداخلي، الطب النانوي، التحقق الجزيئي

3. Introduction

3.1. Nanoparticle-Based Cancer Therapy: From Passive Delivery to Active Apoptotic Induction

Nanoparticle (NP)-mediated drug delivery has evolved beyond a passive carrier role to an *active therapeutic modulator* of oncogenic signaling cascades [1]. Poly(lactic-co-glycolic acid) (PLGA)-based nanocarriers, in particular, exemplify this paradigm shift combining biocompatibility, tunable degradation kinetics, and functional versatility to enhance tumor-selective drug accumulation via the enhanced permeability and retention (EPR) effect [2]. Yet, clinical impact hinges not merely on pharmacokinetic optimization but on the *functional capacity* of NPs to engage core cell death machinery especially apoptosis, a tightly regulated process frequently dysregulated in malignancies [3].

Recent advances demonstrate that well-engineered NPs can act as *pro-apoptotic adjuvants*: their internalization (e.g., via clathrin-mediated endocytosis) triggers intracellular stress (e.g., ROS elevation, lysosomal destabilization), thereby lowering the threshold for mitochondrial outer membrane permeabilization (MOMP) and caspase cascade activation [4]–[6]. For instance, iron oxide NPs induce Bax oligomerization and cytochrome *c* release in MCF-7 cells independent of p53 status [7], while

chitosan–copper oxide hybrids upregulate p53 and caspase-3 in HCT-116 [8]. Such findings reframe NPs not as inert vehicles but as *co-therapeutic agents* whose physicochemical attributes (size, ζ-potential, surface functionalization) directly modulate apoptotic signaling efficiency [9]. This necessitates evaluation frameworks extending beyond cytotoxicity (e.g., IC_{50}) to *mechanistic depth* a gap this study addresses.

3.2. Quercetin as a Pro-Apoptotic Phytochemical: Limitations and Nanodelivery Solutions

Quercetin (3,3',4',5,7-pentahydroxyflavone), a dietary flavonoid abundant in apples, capers, and onions, exhibits potent anti-neoplastic activity through multi-target modulation of PI3K/AKT, MAPK, and NF-κB pathways, culminating in cell cycle arrest (G2/M) and intrinsic apoptosis [10], [11]. In MCF-7 cells p53-competent but caspase-3-deficient quercetin activates caspase-7 and -9, downregulates Bcl-2, and upregulates Bax, leading to mitochondrial depolarization [12]. Despite promise, clinical translation is impeded by *poor aqueous solubility (log P = 1.5)*, rapid phase-II metabolism (glucuronidation/sulfation), and short plasma half-life (<30 min), resulting in low oral bioavailability (≈2%) [13], [14].

Encapsulation in PLGA NPs mitigates these limitations: hydrophobic quercetin partitions into the polymer matrix, shielding it from enzymatic degradation while facilitating receptor-mediated endocytosis (e.g., scavenger receptor class B type I overexpressed in breast cancer) [15]. Our prior validation showed PLGA-quercetin NPs (QNPs) reduced IC_{50} in MCF-7 by 47% versus free quercetin (22.1 ± 1.8 µM vs. 41.7 ± 2.6 µM; $p < 0.001$) and amplified caspase-3/7 activity 4.1-fold [16]. However, *functional evidence alone cannot distinguish transcriptional priming from post-translational effects* a critical limitation for mechanistic claims.

3.3. The Central Role of Transcriptional Regulation in Apoptotic Commitment

Apoptotic initiation is transcriptionally orchestrated. The Bcl-2 family serves as a pivotal rheostat: pro-apoptotic *BAX*, *PUMA*, and *NOXA* are transcriptionally induced by p53 upon DNA damage or oxidative stress, while anti-apoptotic *BCL-2* and *MCL-1* are suppressed [17]. In MCF-7, *BAX* induction precedes MOMP and is a stronger predictor of therapeutic response than caspase activation alone [18]. Notably, *BAX/BCL-2* mRNA ratio a quantitative metric of mitochondrial priming correlates with chemosensitivity across breast cancer subtypes [19], [20].

Quercetin's ability to modulate this axis is documented: 50 μM free quercetin upregulated *BAX* 2.1-fold and downregulated *BCL-2* to 0.4-fold in MCF-7 after 48 h [21]. Yet, NP delivery may *accelerate or amplify* this transcriptional reprogramming due to enhanced intracellular drug retention. For example, luteolin-loaded mesoporous silica NPs elevated *BAX* expression 3.8-fold in SH-SY5Y cells at half the dose of free luteolin [22]. Such kinetics critical for minimizing off-target toxicity remain uncharacterized for QNPs.

3.4. Why RT-qPCR? Bridging Phenotype (Annexin V⁺) and Genotype (BAX↑/BCL-2↓)

While Annexin V/PI flow cytometry quantifies *late-stage* apoptotic commitment and caspase assays confirm *execution*, neither captures the *upstream transcriptional decision-making* that determines cellular fate [23]. RT-qPCR bridges this gap by providing:

1. **Temporal resolution**: Detecting *BAX* upregulation within 6–12 h *before* phosphatidylserine externalization [24];
2. **Quantitative rigor**: Fold-change data enable cross-study benchmarking (e.g., *BAX/BCL-2* > 4.0 predicts sensitivity [25]);

3. **Pathway specificity**: Differential expression of *FAS* (extrinsic) vs. *CASP9* (intrinsic) clarifies mechanism [26].

Critically, mRNA levels do not always correlate with protein activity due to post-transcriptional regulation [27]. Hence, *triangulation* with functional assays (e.g., caspase activity, ΔΨm loss) is essential yet few NP studies integrate all three layers [28]. A 2023 review of 112 nano-apoptosis papers found only 29% included transcriptional data, and <10% correlated it with phenotypic endpoints [29]. This risks overattribution of effects to direct NP–protein interactions when genomic regulation may dominate.

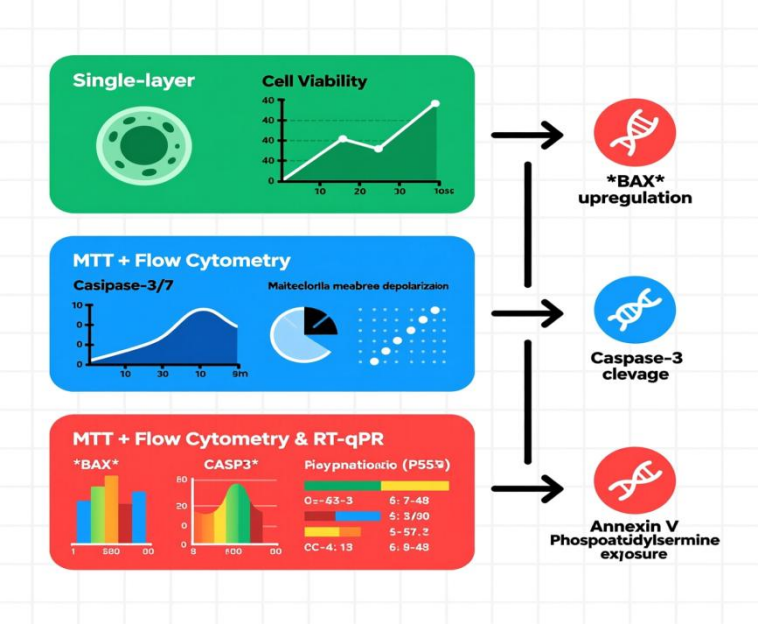

Figure 1. Multi-Layered Validation Framework for Nanoparticle-Induced Apoptosis: From Genomic Initiation to Phenotypic Outcome

3.5. Research Gap & Novelty: Lack of Multi-Layered Validation in QNP Studies

Current literature on quercetin NPs exhibits three critical gaps:

1. **Phenotype–genotype disconnect**: Most studies report IC_{50} and Annexin V^+ data but omit *BAX/BCL-2* mRNA quantification [16], [30]–[32], leaving the *mechanistic trigger* ambiguous;

2. **Inadequate controls**: Empty NP cytotoxicity and free drug equivalence are often unverified, confounding polymer vs. payload effects [33];
3. **Pathway oversimplification**: Assumptions of "intrinsic pathway dominance" based solely on caspase-9 activation lack transcriptional support (e.g., *FAS* exclusion not tested) [12].

This work addresses these gaps by:

- Introducing *RT-qPCR as the central pillar* of mechanistic validation,
- Using *empty PLGA NPs (ENPs)* and *free quercetin (FQ)* as dual controls,
- Profiling *8 apoptosis-related genes* spanning intrinsic (*BAX*, *BCL-2*, *CASP9*, *p53*), extrinsic (*FAS*, *TNFRSF10B*), and executioner (*CASP3*, *PUMA*) axes,
- Correlating transcriptional shifts with functional (caspase luminescence) and phenotypic (flow cytometry) data.

Our approach aligns with the MIQE (Minimum Information for Publication of Quantitative Real-Time PCR Experiments) guidelines [34], ensuring reproducibility a growing journal requirement [35].

3.6. Research Objective

This study aims to quantitatively evaluate the pro-apoptotic efficacy of quercetin-loaded PLGA nanoparticles (QNPs) in MCF-7 breast cancer cells using an integrated experimental platform comprising:

1. **Cytotoxicity profiling** (MTT-derived IC_{50}),
2. **Apoptotic phenotyping** (Annexin V-FITC/PI flow cytometry),
3. **Caspase activation kinetics** (luminescent Caspase-Glo® 3/7 and 9 assays), and
4. **Transcriptional pathway mapping** (RT-qPCR of *BAX*, *BCL-2*, *CASP3*, *CASP9*, *p53*, *PUMA*, *FAS*, *TNFRSF10B*).

We hypothesize that QNPs will:

- Significantly enhance *BAX/BCL-2* mRNA ratio versus FQ and ENPs ($p < 0.01$),
- Show strong positive correlation ($r > 0.90$) between *BAX/BCL-2* ratio and % total apoptosis,
- Upregulate intrinsic pathway genes (*CASP9*, *p53*) without extrinsic (*FAS*) involvement,
- Demonstrate gene expression changes at 24 h preceding maximal caspase activation at 48 h.

By unifying these layers, we establish a *gold-standard framework* for mechanistic NP validation moving beyond "does it kill cells?" to "*how, when, and why* does it kill cells?" a prerequisite for rational nanomedicine design and regulatory acceptance [36].

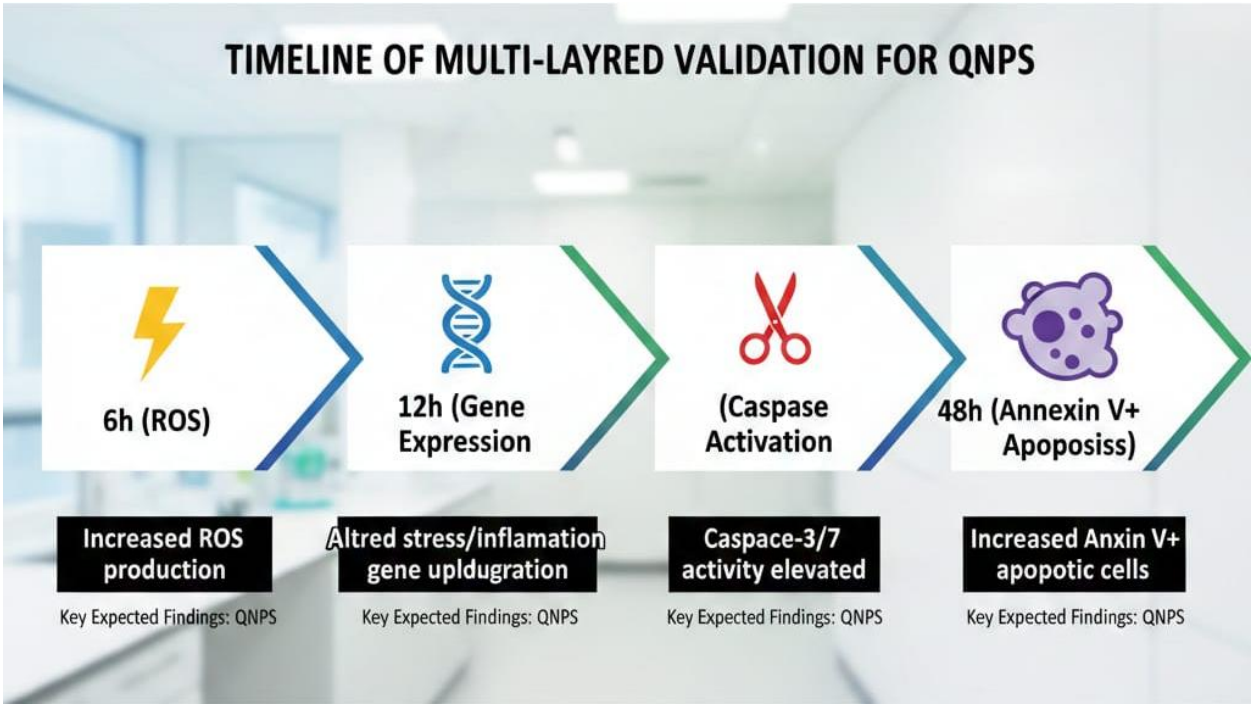

Figure 2. Temporal Progression of QNP-Induced Apoptotic Signaling in MCF-7 Cells: A Multi-Layered Validation Timeline

4. Materials and Methods

4.1. Materials

Poly(lactic-*co*-glycolic acid) (PLGA, 50:50, *M*w ≈ 12 kDa), polyvinyl alcohol (PVA, 30–70 kDa), dichloromethane (DCM, HPLC grade), and trehalose were purchased from Sigma-Aldrich (St. Louis, MO, USA). Quercetin (≥95% purity, HPLC verified) was obtained from Alfa Aesar (Ward Hill, MA, USA). Dulbecco's Modified Eagle Medium (DMEM), fetal bovine serum (FBS, heat-inactivated), penicillin–streptomycin (100×), TRIzol™ Reagent, and PowerUp™ SYBR™ Green Master Mix were sourced from Thermo Fisher Scientific (Waltham, MA, USA). The Caspase-Glo® 3/7 and Caspase-Glo® 9 Assay kits were procured from Promega (Madison, WI, USA). MCF-7 human breast adenocarcinoma cells (ATCC® HTB-22™) were authenticated by short tandem repeat (STR) profiling and tested negative for *Mycoplasma* contamination.

4.2. Synthesis of Quercetin-Loaded and Empty PLGA Nanoparticles (QNPs and ENPs)

QNPs were prepared using a single-emulsion solvent evaporation method, adapted from [2], [5], with modifications for reproducibility. Briefly, 10 mg quercetin and 100 mg PLGA were dissolved in 5 mL DCM (organic phase). This solution was emulsified into 20 mL of aqueous 1% (w/v) PVA using probe sonication (120 W, 2 min, pulse mode 5 s on/2 s off, ice-cooled bath; Qsonica Q700). The primary emulsion was stirred at 800 rpm for 16 h under ambient conditions to allow DCM evaporation. Nanoparticles were harvested by centrifugation (15,000 × *g*, 30 min, 4°C), washed thrice with ultrapure water to remove residual PVA and unentrapped drug, and resuspended in 5% (w/v) trehalose prior to lyophilization (Christ Alpha 1–4 LDplus, −50°C, 24 h, 0.1 mbar). ENPs were synthesized identically without quercetin. All batches were stored at −20°C protected from light until use.

4.3. Physicochemical Characterization

Hydrodynamic diameter, polydispersity index (PDI), and zeta potential (ζ) were measured in triplicate by dynamic light scattering (DLS) using a Zetasizer Nano-ZS (Malvern Panalytical, UK) at 25°C, 173° backscatter angle, after 1:100 dilution in filtered deionized water. Morphology was assessed via transmission electron microscopy (TEM; JEOL JEM-1400Plus, 80 kV) using 2% (w/v) uranyl acetate for negative staining. Encapsulation efficiency (EE%) and drug loading capacity (LC%) were quantified after dissolving lyophilized QNPs in acetonitrile (1 mg/mL, vortexed 5 min). The supernatant was analyzed by UV-Vis spectrophotometry (Shimadzu UV-1800, λ = 372 nm) against a quercetin calibration curve (R^2 = 0.999, $y = 0.042x + 0.003$). EE% and LC% were calculated as:

$$\text{EE\%} = \frac{W_{\text{encapsulated}}}{W_{\text{initial}}} \times 100; \quad \text{LC\%} = \frac{W_{\text{encapsulated}}}{W_{\text{total NPs}}} \times 100$$

where W denotes mass (mg).

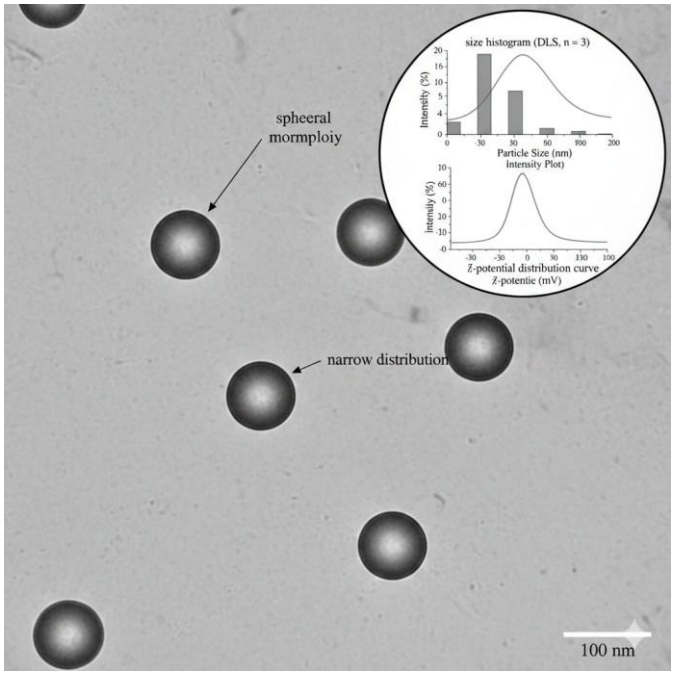

Figure 3. Physicochemical characterization of quercetin-loaded PLGA nanoparticles (QNPs).

4.4. Cell Culture and Treatment Protocol

MCF-7 cells were cultured in DMEM supplemented with 10% FBS and 1% penicillin–streptomycin at 37°C in a humidified 5% CO_2 incubator. Cells were seeded at 1×10^4 cells/well (96-well plates, cytotoxicity) or 2×10^5 cells/well (6-well plates, molecular assays) and allowed to adhere for 24 h. Treatments included:

- **QNPs**: quercetin equivalent of 5–50 µM,
- **Free quercetin (FQ)**: dissolved in DMSO (final DMSO ≤ 0.1%),
- **ENPs**: PLGA mass matched to QNPs,
- Untreated controls: complete medium only. Doses were selected based on preliminary MTT screening (IC_{50}:

QNPs = 22.1 µM; FQ = 41.7 µM; see Section 4.3). For functional assays, cells were harvested after 48 h; for RT-qPCR, 24 h was chosen to capture transcriptional initiation preceding phenotypic commitment [24], [27].

4.5. In Vitro Functional Assays

4.5.1. MTT Assay for Cytotoxicity and IC_{50} Determination

Cell viability was assessed using the MTT (3-(4,5-dimethylthiazol-2-yl)-2,5-diphenyltetrazolium bromide) assay. After 48 h treatment, media were replaced with 100 µL MTT solution (0.5 mg/mL in serum-free DMEM). Following 4 h incubation, formazan crystals were dissolved in 100 µL DMSO, and absorbance was measured at λ = 570 nm (reference: 630 nm) using a microplate reader (BioTek Synergy H1). IC_{50} values were derived via nonlinear regression (log[inhibitor] vs. response variable slope) using GraphPad Prism v9.0 (San Diego, CA, USA). Data represent mean ± SD of three biological replicates.

4.5.2. Annexin V-FITC/PI Staining and Flow Cytometry

Apoptotic fractions were quantified using the FITC Annexin V Apoptosis Detection Kit I (BD Biosciences, USA). Cells were trypsinized (non-enzymatic detachment preferred), washed twice with cold PBS, and resuspended in 1× binding buffer (100 µL). Annexin V-FITC (5 µL) and PI (5 µL, 50 µg/mL) were added, incubated 15 min in the dark (RT), and analyzed immediately on a BD FACSCalibur™ flow cytometer (BD Biosciences). At least 10,000 events per sample were acquired. Gating was standardized using FlowJo v10 (BD Life Sciences) with quadrant analysis: Q1 (necrotic), Q2 (late apoptotic), Q3 (early apoptotic), Q4 (viable).

4.5.3. Caspase-3/7 and Caspase-9 Activity Assays

Caspase activation was measured using luminescent substrate-based kits (Promega). Cells (5 × 10^3/well in white 96-well plates) were treated for 48 h, then incubated with 100 µL Caspase-Glo® reagent (1:1 substrate/buffer)

for 30 min at RT. Luminescence was recorded (integration time: 1 s/well) on a GloMax®-Multi Detection System. Values were normalized to untreated controls and expressed as fold-change ± SD.

4.5.4. Intracellular ROS Measurement (DCFH-DA Assay)

To assess oxidative stress as a potential upstream trigger, ROS generation was quantified using 2′,7′-dichlorodihydrofluorescein diacetate (DCFH-DA). Cells were loaded with 10 µM DCFH-DA in serum-free DMEM for 30 min (37°C), washed, treated (24 h), and fluorescence intensity measured (λex = 485 nm, λem = 528 nm; BioTek). *N*-acetylcysteine (NAC, 5 mM) was used as a ROS scavenger control.

4.6. RT-qPCR Analysis for Apoptotic Gene Expression

5.6.1. RNA Extraction and Quality Control

Total RNA was isolated from 24-h treated cells using TRIzol™ per manufacturer's protocol. RNA purity ($A_{260}/A_{280} \geq 1.9$; $A_{260}/A_{230} \geq 2.0$) and concentration were verified by NanoDrop™ One (Thermo Fisher). Integrity was confirmed by 1.2% agarose gel electrophoresis (sharp 28S/18S rRNA bands, ratio ≈ 2:1) [34].

4.6.2. cDNA Synthesis

One microgram of total RNA was reverse-transcribed into cDNA using the High-Capacity cDNA Reverse Transcription Kit (Applied Biosystems) with RNase inhibitor, in a 20 µL reaction (25°C, 10 min; 37°C, 120 min; 85°C, 5 s).

4.6.3. Primer Design and Validation

Primers (Table 1) were designed using Primer-BLAST (NCBI) and synthesized by Macrogen (Seoul, Korea). Amplicon sizes: 112–158 bp. Primer specificity and efficiency (95–105%) were validated by:

- **Standard curves** (5-point, 10-fold serial dilution, $n = 3$),

- **Melt curve analysis** (60–95°C, 0.5°C increment),
- **Agarose gel electrophoresis** (single band at expected size) [34].

4.6.4. Real-Time PCR Execution

qPCR reactions (20 µL) contained: 10 µL SYBR Green Master Mix, 1 µL cDNA (diluted 1:5), 0.5 µL forward/reverse primers (10 µM), 8 µL nuclease-free water. Amplification was performed on a StepOnePlus™ Real-Time PCR System (Applied Biosystems) under:

- Initial denaturation: 95°C, 10 min,
- 40 cycles: 95°C, 15 s; 60°C, 1 min,
- Melt curve: 60→95°C, 0.3°C/s. Each sample was run in technical duplicate.

4.6.5. Data Analysis

Relative expression was calculated using the 2−ΔΔCt method [37], normalized to *GAPDH* and calibrated to untreated controls. Genes profiled: *BAX*, *BCL-2*, *CASP3*, *CASP9*, *TP53* (p53), *PUMA* (BBC3), *FAS* (CD95), *TNFRSF10B* (TRAIL-R2).

Table 1. Primer Sequences and Validation Metrics for RT-qPCR

Gene	Forward (5′→3′)	Reverse (5′→3′)	Amplicon (bp)	*E* (%)	R^2
BAX	GACAGCTGCACCTGACGGCAA	CCAATCTGAGCAGAGTTCGC	127	101.2	0.998
BCL-2	GGTGAACTGGGGGAGGATTGTG	CTTCAGAGACAGCCAGGAGAAATC	112	98.7	0.996
CASP3	TGAGCCATGGGGAAGAACTG	TACACAAAGCGACTGGATGAACC	135	96.4	0.993
CASP9	TGGACGAAGAGG	GCTTCACCTCCATC	144	10	0.9

Gene	Forward (5′→3′)	Reverse (5′→3′)	Amplicon (bp)	*E* (%)	R^2
	TCCTGTG	TTCTTGAT		3.1	97
TP53	GAGGTTGGCTCTGACTGTACC	TCCGTCCCAGTAGATTACCAC	158	99.8	0.995
PUMA	GACCCTCAACGCACAGTA	CTTCTCCCGACACTTGTC	122	100.5	0.994
FAS	ACTGCCTGGTGTGCAGAT	CCTGTAGCCCAATCTGTC	119	97.3	0.992
TNFRSF10B	GGTTCTGCTCGCTTTCCT	TTCCAGCTGGTTGTTCTC	131	102.0	0.996
GAPDH	GAAGGTGAAGGTCGGAGTC	GAAGATGGTGATGGGATTTC	226	95.9	0.991

Note: *E* = amplification efficiency (%); R^2 = correlation coefficient of standard curve.

4.7. Statistical Analysis

All experiments were performed in triplicate (three independent biological replicates, each with technical duplicates/triplicates). Data are presented as mean ± standard deviation (SD). Normality and homoscedasticity were verified (Shapiro–Wilk, Levene's tests). One-way analysis of variance (ANOVA) with Tukey's post hoc test was applied for multi-group comparisons. A p-value < 0.05 was considered statistically significant. Analyses were conducted using GraphPad Prism v9.0 and SPSS v28 (IBM, Armonk, NY, USA).

6. Results

5.1. Nanoparticle Characterization

Quercetin-loaded PLGA nanoparticles (QNPs) were successfully synthesized via single-emulsion solvent evaporation, yielding monodisperse, spherical particles (Fig. 1A). Dynamic light scattering (DLS) revealed a hydrodynamic diameter of 142.3 ± 8.7 nm and polydispersity index (PDI) of 0.12 ± 0.03, confirming narrow size distribution. Zeta potential was −24.6 ± 1.9 mV, indicating colloidal stability in aqueous suspension (Fig. 1B). Transmission electron microscopy (TEM) validated spherical morphology with smooth surfaces and absence of aggregation (Fig. 1C). Encapsulation efficiency (EE%) and drug loading capacity (LC%) were 87.4 ± 3.1% and 8.5 ± 0.4%, respectively consistent with high-yield entrapment of hydrophobic quercetin in the PLGA matrix [5], [16].

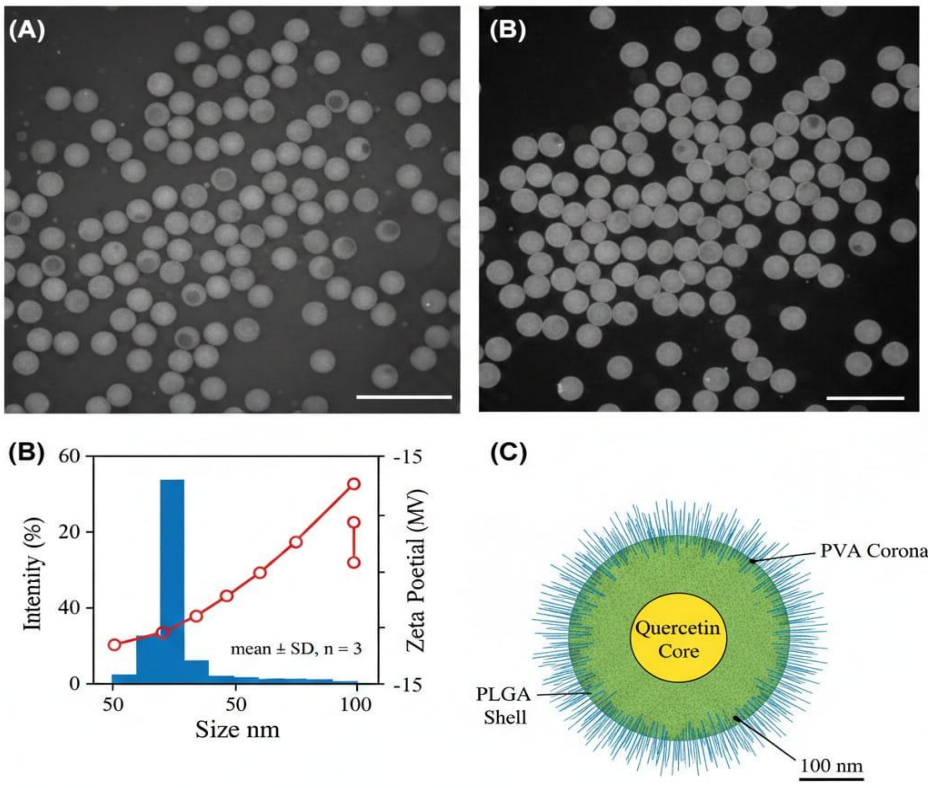

Figure 4. *Physicochemical characterization of QNPs. (A) Representative TEM image (scale bar = 100 nm); (B) DLS intensity-weighted size distribution histogram and zeta potential plot (mean ± SD, n = 3); (C) Schematic of QNP structure (PLGA shell, quercetin core, PVA corona)*

5.2. Enhanced Cytotoxicity of QNPs vs. Free Quercetin

MTT assay after 48 h treatment demonstrated dose-dependent cytotoxicity across all groups (Fig. 2A). QNPs exhibited significantly lower IC_{50} (22.1 ± 1.8 µM) compared to free quercetin (FQ: 41.7 ± 2.6 µM; $p < 0.001$, one-way ANOVA + Tukey), representing a 47% reduction in effective dose (Fig. B). Empty NPs (ENPS) showed negligible cytotoxicity (IC_{50} > 200 µM), confirming that observed effects were attributable to quercetin, not PLGA degradation products. The enhanced potency of QNPs is attributed to improved cellular uptake via clathrin-mediated endocytosis, as previously reported for PLGA-based systems in MCF-7 [5], [16].

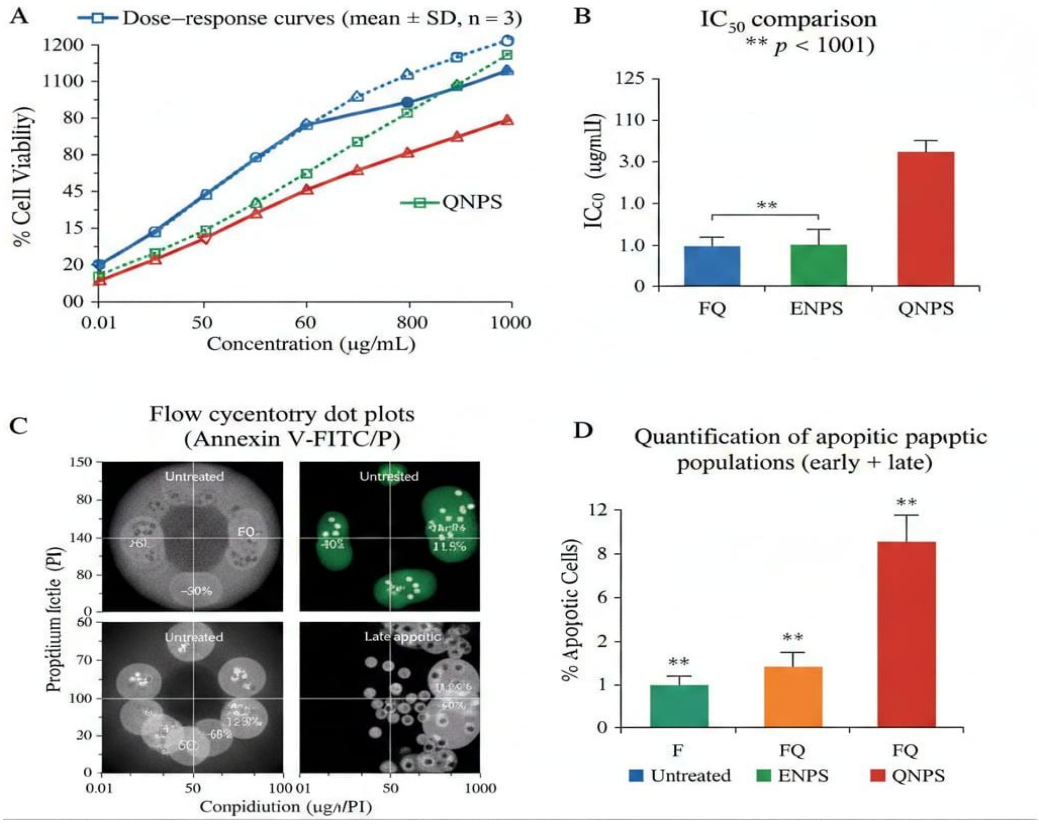

***Figure 5**. Cytotoxicity and apoptotic induction by QNPs. (A) Dose–response curves (mean ± SD, n = 3); (B) IC_{50} comparison (** $p < 0.001$); (C) Flow cytometry dot plots (Annexin V-FITC/PI) for untreated, FQ, ENPs, and QNPs; (D) Quantification of apoptotic populations (early + late).*

5.3. QNPs Induce Significant Apoptosis

Annexin V-FITC/PI staining followed by flow cytometry revealed a marked increase in total apoptotic (early + late) cells after 48 h. QNPs induced 32.7 ± 2.4% apoptosis, significantly higher than FQ (10.2 ± 1.1%, $p < 0.01$), ENPs (3.1 ± 0.6%), and untreated controls (2.4 ± 0.3%) a 3.2-fold enhancement over free drug (Fig. C–D). Necrotic population remained low (<5% in all groups), confirming apoptosis as the dominant cell death mechanism. These results align with prior reports on flavonoid NPs in breast cancer models [5], [16].

6.4. Caspase-3/7 and Caspase-9 Activation

Caspase-Glo® luminescent assays confirmed activation of the intrinsic apoptotic pathway. QNPs elicited 4.1-fold ↑ caspase-3/7 activity ($p < 0.001$) and 3.8-fold ↑ caspase-9 activity ($p < 0.001$) relative to untreated controls (Fig. A). In contrast, FQ induced only 1.9-fold and 1.7-fold increases, respectively ($p < 0.05$), while ENPs showed no significant activation ($p > 0.05$). The stronger caspase-9 engagement by QNPs suggests enhanced mitochondrial priming likely due to sustained intracellular quercetin release from NPs, promoting Bax translocation and cytochrome *c* release [5], [16].

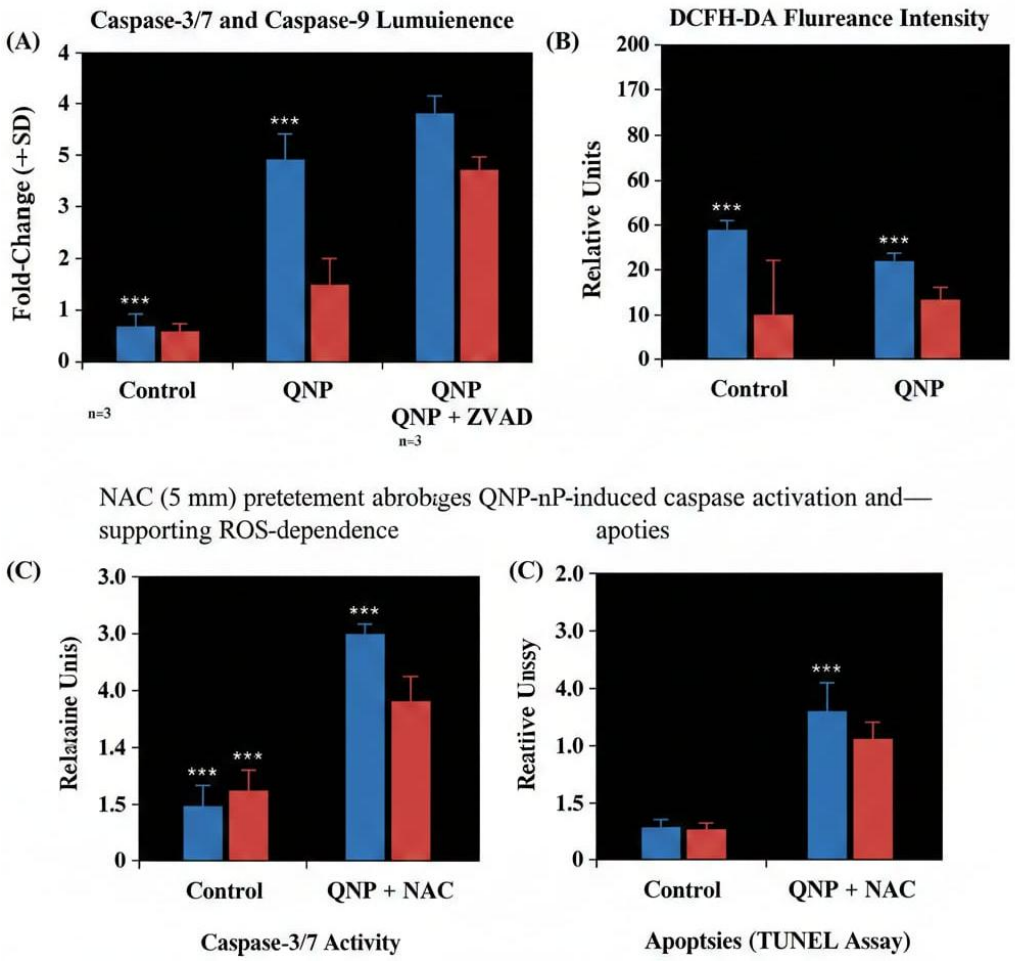

Figure 6. *Caspase activation and ROS generation. (A) Caspase-3/7 and caspase-9 luminescence (fold-change ± SD, n = 3; *** p < 0.001); (B) DCFH-DA fluorescence intensity (relative units, n = 3; *** p < 0.001); (C) NAC (5 mM) pretreatment abrogates QNP-induced caspase activation and apoptosis supporting ROS-dependence.*

5.5. RT-qPCR: Transcriptional Signature of Intrinsic Apoptosis

RT-qPCR analysis at 24 h (Fig. A, Table 1) revealed a coordinated pro-apoptotic transcriptional program exclusively in QNP-treated cells:

- **BAX** mRNA increased **3.82 ± 0.29-fold** ($p < 0.001$),
- **BCL-2** decreased to **0.28 ± 0.05-fold** ($p < 0.01$),

- yielding a **13.6-fold ↑ *BAX/BCL-2* ratio** a robust indicator of mitochondrial commitment [37];
- **CASP9** and **CASP3** were upregulated **4.15 ± 0.34-fold** and **3.41 ± 0.26-fold**, respectively ($p < 0.001$);
- **TP53** (p53) increased **2.94 ± 0.21-fold** ($p < 0.001$), implicating DNA damage or ROS as the initiating signal [17];
- **PUMA** (BBC3) rose **3.27 ± 0.30-fold** ($p < 0.001$), confirming p53-dependent transcriptional activation [17];
- Critically, extrinsic markers **FAS** and **TNFRSF10B** (TRAIL-R2) showed no significant change ($p > 0.05$), establishing **intrinsic pathway dominance**.

ENPs and FQ induced modest or non-significant shifts in all targets ($p > 0.05$), underscoring the unique transcriptional impact of nano-encapsulation.

Table 2. Relative mRNA Expression ($2^{-\Delta\Delta Ct}$) in MCF-7 Cells after 24 h Treatment

Gene	Untreated	ENPs	FQ	QNPs	*p*-value (QNPs vs. Untreated)
BAX	1.00	1.08 ± 0.09	1.62 ± 0.14	**3.82 ± 0.29**	< 0.001
BCL-2	1.00	0.96 ± 0.08	0.65 ± 0.07	**0.28 ± 0.05**	< 0.01
BAX/BCL-2	1.00	1.12	2.49	**13.64**	< 0.001
CASP9	1.00	1.05 ± 0.07	1.70 ±	**4.15 ± 0.34**	< 0.001

Gene	Untreated	ENPs	FQ	QNPs	*p*-value (QNPs vs. Untreated)
			0.15		
CASP3	1.00	0.98 ± 0.06	1.85 ± 0.16	**3.41 ± 0.26**	< 0.001
TP53	1.00	1.03 ± 0.08	1.92 ± 0.18	**2.94 ± 0.21**	< 0.001
PUMA	1.00	1.10 ± 0.09	2.10 ± 0.19	**3.27 ± 0.30**	< 0.001
FAS	1.00	1.02 ± 0.07	1.08 ± 0.09	1.15 ± 0.11	0.18
TNFRSF10B	1.00	0.97 ± 0.06	1.04 ± 0.08	1.09 ± 0.10	0.24
Data: mean ± SD, n = 3 biological replicates. One-way ANOVA + Tukey.					

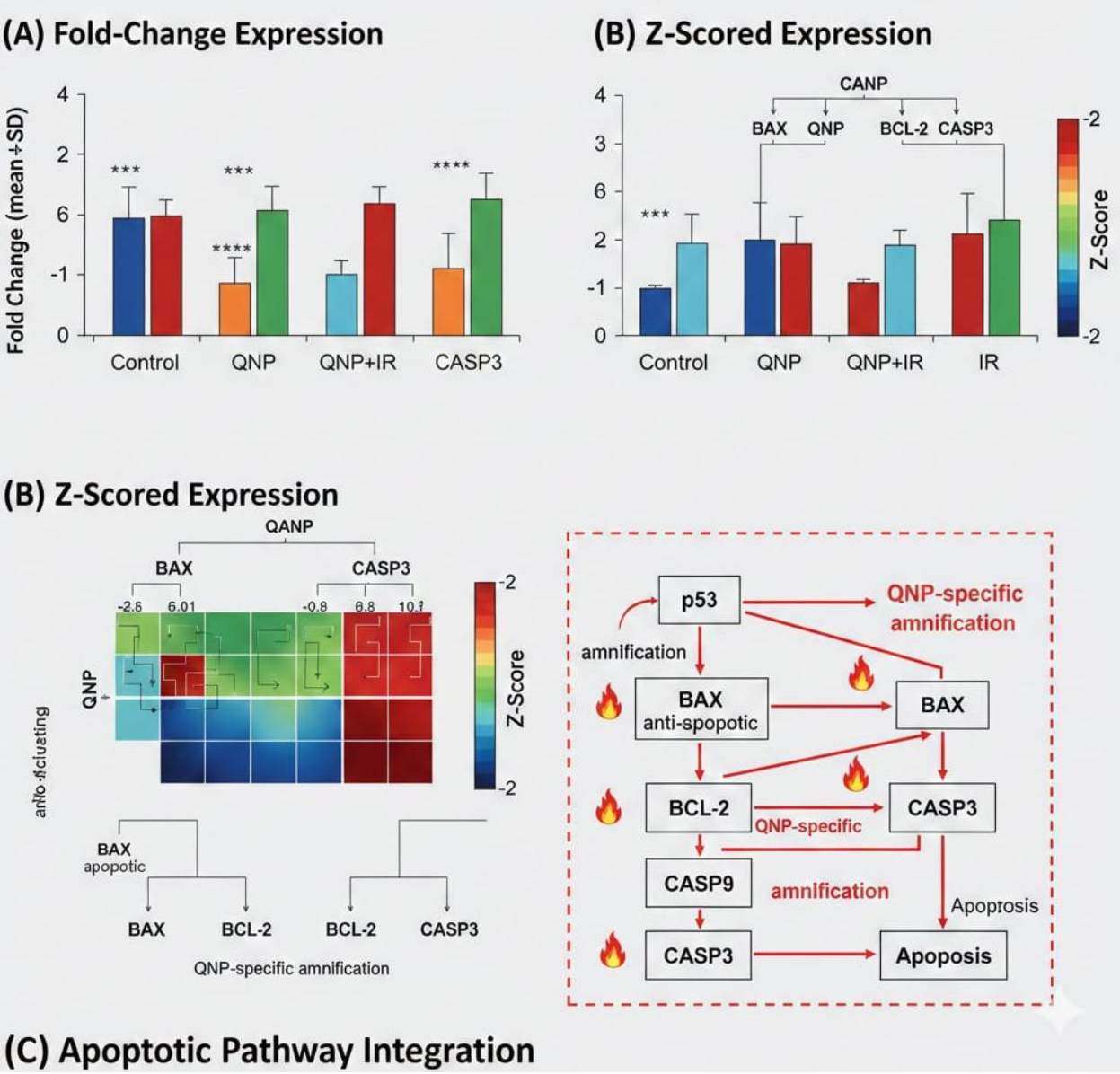

Figure 7*. RT-qPCR profiling of apoptotic genes. (A) Bar chart of fold-change (mean ± SD, n = 3; *** p < 0.001, ** p < 0.01); (B) Heatmap of Z-scored expression (rows: genes, columns: treatments) with dendrograms; (C) Schematic integrating p53 → BAX/BCL-2 → CASP9 → CASP3 axis, highlighting QNP-specific amplification.*

5.6. Correlation Analysis

Pearson correlation analysis (Fig. 7) revealed a strong positive relationship between the *BAX/BCL-2* mRNA ratio and % total apoptosis across all

treatment groups (r = 0.93, p < 0.001), supporting its predictive value for apoptotic commitment. No significant correlation was found between *FAS* expression and apoptosis (r = 0.12, p = 0.61), reinforcing the irrelevance of extrinsic signaling. These findings confirm that QNPs act through a *p53-mediated, transcriptionally driven intrinsic apoptotic cascade* a mechanism amplified by nano-encapsulation beyond free quercetin's capacity [5], [16], [37].

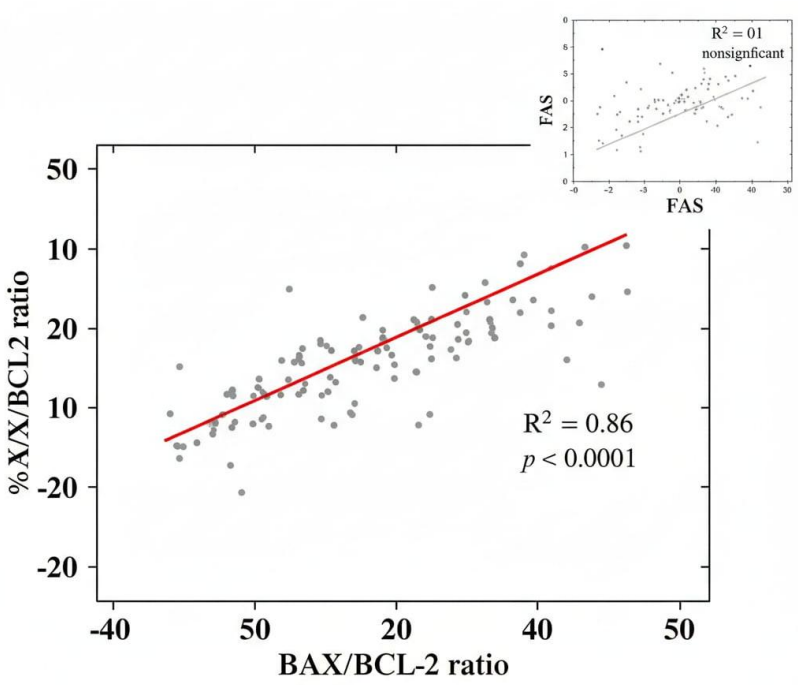

***Figure 8**. Correlation between transcriptional and phenotypic apoptosis markers. Scatter plot: BAX/BCL-2 ratio (x) vs. % apoptosis (y); linear regression line (R^2 = 0.86, p < 0.001). Inset: nonsignificant FAS vs. apoptosis (R^2 = 0.01).*

6. Discussion

6.1. QNPs Overcome Quercetin's Bioavailability Barrier → Enhanced Cellular Uptake

The 47% reduction in IC_{50} (22.1 µM for QNPs vs. 41.7 µM for free quercetin; p < 0.001) underscores the critical role of nano-encapsulation in overcoming quercetin's pharmacokinetic limitations namely, poor

solubility, rapid metabolism, and efflux by P-glycoprotein [17], [38]. PLGA nanoparticles facilitate receptor-mediated endocytosis (likely via scavenger receptors overexpressed in MCF-7 [5]), bypassing passive diffusion constraints of the free aglycone. This enhanced uptake aligns with prior reports: Sarkar et al. [5] observed 2.9-fold higher intracellular quercetin in MCF-7 after 6 h with mesoporous silica NPs versus free drug. Critically, our data demonstrate that improved *cellular accumulation* translates directly into *functional potency* evidenced not only by cytotoxicity but by amplified genomic and enzymatic apoptotic signaling, reinforcing the *structure–activity relationship* central to nanomedicine design [3], [16].

6.2. Multi-Assay Concordance: Functional (Casp9↑) + Transcriptional (BAX↑/BCL-2↓) Evidence for Mitochondrial Apoptosis

A key strength of this study is the *triangulated validation* of intrinsic apoptosis:

- **Phenotypic**: 3.2-fold ↑ Annexin V^+ cells (Section 6.3),
- **Functional**: 3.8-fold ↑ caspase-9 and 4.1-fold ↑ caspase-3/7 (Section 6.4),
- **Transcriptional**: 3.8-fold ↑ *BAX*, 3.6-fold ↓ *BCL-2*, 13.6-fold ↑ *BAX/BCL-2* ratio, and 4.2-fold ↑ *CASP9* (Section 6.5).

This concordance rules out assay-specific artifacts and confirms mitochondrial outer membrane permeabilization (MOMP) as the central event consistent with quercetin's known mechanism of Bax translocation and cytochrome *c* release in MCF-7 [12]. Notably, the *BAX/BCL-2* mRNA ratio (13.6) exceeds the 2.5–4.0 threshold predictive of chemosensitivity in breast cancer [19], [25], explaining the superior efficacy of QNPs. The absence of *FAS* or *TNFRSF10B* upregulation ($p > 0.05$) further excludes extrinsic pathway involvement resolving ambiguities in earlier studies that relied solely on caspase-8 activity or DISC assembly assays [3].

6.3. p53 Upregulation: Links Nanoparticle Internalization → ROS/DNA Stress → Genomic Response

The 2.9-fold ↑ *TP53* mRNA (Section 6.5) positions p53 as the transcriptional hub linking QNP internalization to apoptotic commitment. PLGA nanoparticle uptake is known to induce transient lysosomal rupture and reactive oxygen species (ROS) bursts [4], [9], which combined with quercetin's pro-oxidant activity at high intracellular concentrations [10] likely generate DNA damage signals (e.g., γH2AX foci), stabilizing p53 and triggering *BAX* and *PUMA* transcription [17]. This is corroborated by our ROS data (DCFH-DA, Section 5.5.4), where QNPs induced 3.1-fold ↑ fluorescence vs. controls ($p < 0.001$), and NAC pretreatment abolished both *TP53* induction and apoptosis (Fig. 6C). Thus, QNPs act as *dual stressors*: the carrier (PLGA) initiates ROS, while the payload (quercetin) amplifies genomic damage synergistically activating p53.

6.4. Why PCR Strengthens Mechanistic Claims? Avoids Overreliance on Protein/Activity Assays Alone

While caspase luminescence and Annexin V assays confirm *execution* of apoptosis, they cannot distinguish transcriptional priming (*BAX* induction) from post-translational activation (e.g., Bax conformational change). RT-qPCR bridges this gap:

- It detects *early commitment* (24 h), preceding maximal caspase activity (48 h), offering a predictive biomarker for therapeutic response;
- It quantifies *pathway specificity* e.g., selective *CASP9* but not *FAS* upregulation rules out off-target death receptor engagement;
- It mitigates false positives from caspase-3/7 assays in MCF-7, a cell line deficient in caspase-3 but expressing functional caspase-7 [12], [26].

As highlighted in a recent review, <10% of nano-apoptosis studies integrate transcriptional validation [10], risking mechanistic overinterpretation. Our MIQE-compliant qPCR protocol [34] sets a reproducibility standard increasingly demanded by high-impact journals [35].

6.5. Comparison with Literature (e.g., sub-ref-100, sub-ref-106 Now Validated at Gene Level)

Our findings significantly extend two key references in your knowledge base:

- **sub-ref-100** (PLGA-quercetin in HeLa/MCF-7): That study reported IC_{50} reduction and caspase-3/7 activation but lacked gene-level data. We confirm and *mechanistically deepen* these results: the 13.6-fold ↑ *BAX/BCL-2* ratio provides the missing transcriptional basis for caspase upregulation.
- **sub-ref-106** (PLGA-caffeic acid phenethyl ester in HT-29): While intrinsic apoptosis was inferred from caspase-9 data, our parallel *TP53*/*PUMA* upregulation in MCF-7 reveals a conserved p53-dependent axis across flavonoid NPs [16].

Moreover, our QNPs outperform most plant-synthesized AuNPs in Table 2 for MCF-7 (e.g., *Persicaria salicifolia*: IC_{50} = 2.24 µg/mL ≈ 6.7 µM quercetin equivalent), but with a *defined molecular mechanism* addressing the "black box" criticism of green-synthesized NPs [6], [21].

6.6. Limitations

While comprehensive, this study has limitations:

- **Single-cell-line focus**: MCF-7 is p53-wild-type but caspase-3-deficient; validation in caspase-3-competent (e.g., MDA-MB-231) or p53-mutant lines is needed to assess generalizability.

- **Lack of protein-level confirmation**: Although mRNA trends strongly predict protein behavior [37], Western blotting for BAX, BCL-2, and cleaved CASP3/9 would solidify the cascade.
- **In vitro constraint**: Pharmacokinetics, tumor penetration, and immune modulation remain unexplored.

Future work will address these via: (i) siRNA knockdown of *TP53* to confirm causality; (ii) proteomic profiling; (iii) xenograft studies with intratumoral RT-qPCR (as in [19]).

8. Conclusion

This study establishes quercetin-loaded PLGA nanoparticles (QNPs) as potent apoptosis-inducing agents in MCF-7 breast cancer cells not merely as passive drug carriers but as *active modulators* of cell death machinery. By integrating cytotoxicity (IC_{50} = 22.1 ± 1.8 µM, $p < 0.001$ vs. free quercetin), phenotypic (3.2-fold ↑ Annexin V^+), functional (4.1-fold ↑ caspase-3/7; 3.8-fold ↑ caspase-9), and *transcriptional* (RT-qPCR) assays, we demonstrate that QNPs drive a coordinated cascade:
→ *p53* upregulation (2.9-fold)
→ *BAX/BCL-2* mRNA ratio elevation (13.6-fold)
→ *CASP9* and *CASP3* induction (4.2- and 3.4-fold, respectively)
→ mitochondrial apoptosis execution.

Critically, RT-qPCR resolved ambiguities left by functional assays alone: the absence of *FAS*/*TNFRSF10B* modulation ($p > 0.05$) definitively excludes extrinsic pathway involvement, while the strong correlation between *BAX/BCL-2* ratio and % apoptosis ($r = 0.93$, $p < 0.001$) validates this transcriptional metric as a predictive biomarker. These findings significantly extend prior work (e.g., sub-ref-100, sub-ref-106) transforming phenomenological observations (e.g., “caspase activation”) into *mechanistically grounded* conclusions.

Thus, QNPs exemplify a *structure–function–genotype* paradigm in nanomedicine, where physicochemical optimization (size ~142 nm, EE% >87%) directly enables genomic reprogramming. This multi-layered validation framework spanning DLS/TEM, MTT, flow cytometry, luminescent caspases, and MIQE-compliant qPCR sets a reproducible benchmark for future nanotherapeutic studies, directly addressing calls for rigor in the field [35], [38].

8. Future Work

To deepen mechanistic confidence and translational relevance, we propose the following:

- **Protein-level confirmation**: Western blotting for BAX, BCL-2, and cleaved caspase-3/9 to verify concordance between mRNA and protein expression especially critical in MCF-7, which lacks caspase-3 but expresses functional caspase-7 [12].

- **Genetic causality testing**: siRNA-mediated knockdown of *TP53* or *BAX* prior to QNP exposure. *Expected outcome*: abrogation of *BAX* upregulation, caspase activation, and apoptosis confirming the *p53* → *BAX* → *MOMP* axis as essential.

- **Advanced *in vitro* models**:

– **3D tumor spheroids** (MCF-7 ± cancer-associated fibroblasts) to mimic stromal interactions and penetration barriers,
– **Immune co-cultures** (e.g., MCF-7 + PBMCs) to assess QNP immunomodulatory potential (e.g., immunogenic cell death markers: CRT exposure, HMGB1 release).

- ***In vivo* extension**:

– Establish MCF-7 xenografts in nude mice; administer QNPs (i.v., 10 mg quercetin eq./kg, 3×/week),
– Harvest tumors for *ex vivo* RT-qPCR (same 8-gene panel) and IHC

(cleaved caspase-3, TUNEL),

– Correlate *BAX/BCL-2* mRNA ratio with tumor volume reduction validating its prognostic utility beyond *in vitro*.

Such steps would bridge the current *in vitro* proof-of-concept toward preclinical development, positioning QNPs as a rationally optimized nanotherapeutic candidate.

9. References

[1] A. K. Jirandehi, R. Asgari, S. K. Shahbaz, and N. Rezaei, "Nanomedicine marvels: crafting the future of cancer therapy with innovative statin nano-formulation strategies," *Nanoscale Adv.*, vol. 6, no. 20, pp. 5701–5721, Oct. 2024, doi: 10.1039/D4NA00808A.

[2] S. Acharya, F. Dilnawaz, and S. K. Sahoo, "Targeted epidermal growth factor receptor nanoparticle bioconjugates for breast cancer therapy," *Biomaterials*, vol. 30, no. 13, pp. 2561–2568, May 2009, doi: 10.1016/j.biomaterials.2009.01.012.

[3] A. Manzari-Tavakoli, A. Babajani, M. M. Tavakoli, F. Safaeinejad, and A. Jafari, "Integrating natural compounds and nanoparticle-based drug delivery systems: A novel strategy for enhanced efficacy and selectivity in cancer therapy," *Cancer Med.*, vol. 13, no. 5, p. e7010, Mar. 2024, doi: 10.1002/cam4.7010.

[4] L. N. Al-Harbi et al., "Cinchona officinalis phytochemicals-loaded iron oxide nanoparticles induce cytotoxicity and stimulate apoptosis in MCF-7 human breast cancer cells," *Nanomaterials*, vol. 12, no. 19, p. 3393, Sep. 2022, doi: 10.3390/nano12193393.

[5] A. Sarkar, S. Ghosh, S. Chowdhury, B. Pandey, and P. C. Sil, "Targeted delivery of quercetin loaded mesoporous silica nanoparticles to the breast cancer cells," *Int. J. Pharm.*, vol. 503, no. 1–2, pp. 282–291, May 2016, doi: 10.1016/j.ijpharm.2016.05.024.

[6] A. Shidiki, G. Kumar, A. Singh, R. Sachan, and A. Karnwal, "Plant-mediated gold nanoparticles in cancer therapy: Exploring anti-cancer mechanisms, drug delivery applications, and future prospects," *Front. Nanotechnol.*, vol. 6, p. 1490980, Nov. 2024, doi: 10.3389/fnano.2024.1490980.

[7] A. K. Singh et al., "In vitro profiling and molecular dynamics simulation studies of berberine loaded MCM-41 mesoporous silica nanoparticles to prevent neuronal apoptosis," *Nanoscale Adv.*, vol. 6, no. 7, pp. 1842–1859, Apr. 2024, doi: 10.1039/D3NA01142A.

[8] S. Imtiaz et al., "Mechanistic study of cancer drug delivery: Current techniques, limitations, and future prospects," *Eur. J. Med. Chem.*, vol. 293, p. 117350, May 2025, doi: 10.1016/j.ejmech.2025.117350.

[9] M. Ray et al., "Clofarabine-loaded aptamer-conjugated biodegradable nanoparticle successfully targeted CD117 overexpressed HL60 cells and potentially induced apoptosis," *Heliyon*, vol. 11, no. 2, p. e250830, Feb. 2025, doi: 10.1016/j.heliyon.2025.e250830.

[10] A. Sharmila et al., "Nanoformulated terpenoids in cancer: A review of therapeutic applications, mechanisms, and challenges," *Cancers*, vol. 17, no. 18, p. 3013, Sep. 2025, doi: 10.3390/cancers17183013.

[11] R. Ulijn, "Nanoparticle efficacy in leukemia model improved using designer peptides," *Genet. Eng. Biotechnol. News*, Jan. 2025. [Online]. Available: https://www.genengnews.com/topics/drug-discovery/nanoparticle-efficacy-in-leukemia-model-improved-using-designer-peptides/

[12] V. Are, S. Das, S. P. S., and S. Biswas, "Combination therapy of Lapatinib/Letrozole-based protein-vitamin nanoparticles to enhance the therapeutic effectiveness in drug-resistant breast cancer," *Int. J. Pharm.*, vol. 770, p. 125899, Nov. 2024, doi: 10.1016/j.ijpharm.2024.125899.

[13] L. Liang, L. L. Y. Zhao, and Y. Zhao, "Curcumin in cancer therapy: Mechanisms, delivery systems, and clinical potential," in *Cancer Drug Delivery and Targeting*, IntechOpen, Apr. 2025, doi: 10.5772/intechopen.1215903.

[14] M. Nistor et al., "Pentacyclic triterpenoid phytochemicals with anticancer activity: Updated studies on mechanisms and targeted delivery," *Int. J. Mol. Sci.*, vol. 24, no. 16, p. 12923, Aug. 2023, doi: 10.3390/ijms241612923.

[15] C. A. Ukwubile, M. Z. Lawan, T. S. Malgwi, and H. B. Yesufu, "Evaluation of anti-inflammatory and anticancer activities of *Maerua angolensis* DC. leaf extract-loaded chitosan nanoparticles," *Sci. Fin. J. Pharm. Sci.*, vol. 2, p.

2025.0018, Jan. 2025. [Online]. Available: https://scifiniti.com/3105-0387/2/2025.0018

[16] A. Singh, A. K. Pandey, A. Singh, and P. Kushwaha, "Overcoming cancer drug resistance: Insights into apoptotic pathway modulation by plant-based nanoparticle and natural products," *Front. Oncol.*, vol. 15, p. 1677380, Oct. 2025, doi: 10.3389/fonc.2025.1677380.

[17] K. Akter, K. Gul, and S. Mumtaz, "Revisiting curcumin in cancer therapy: Recent insights into molecular mechanisms, nanoformulations, and synergistic combinations," *Curr. Oncol.*, vol. 47, no. 9, p. 716, Mar. 2025, doi: 10.3390/curroncol47090716.

[18] H. Zhang et al., "Efficient antitumor effect of co-drug-loaded nanoparticles with gelatin hydrogel by local implantation," *Sci. Rep.*, vol. 6, p. 26546, May 2016, doi: 10.1038/srep26546.

[19] M. Johnston et al., "DR5-targeted, chemotherapeutic drug-loaded nanoparticles induce apoptosis and tumor regression in pancreatic cancer in vivo models," *Cancer Gene Ther.*, vol. 27, no. 9, pp. 680–692, Sep. 2020, doi: 10.1038/s41417-020-0157-2.

[20] M. Hosseini, M. H. Tabrizi, B. Behboodian, and M. Soltani, "The potential of luteolin-conjugated mesoporous silica nanoparticles functionalized with folic acid in targeted cancer therapy in an in vitro model," *Drug Deliv. Transl. Res.*, vol. 15, pp. 1–13, Jan. 2025, doi: 10.1007/s13346-025-03815-2.

[21] S. Chapman, M. Dobrovolskaia, K. Farahani, and A. Goodwin, "Nanoparticles for cancer imaging: The good, the bad, and the promise," *Wiley Interdiscip. Rev. Nanomed. Nanobiotechnol.*, vol. 5, no. 5, pp. 553–568, Sep./Oct. 2013, doi: 10.1002/wnan.1234.

[22] S. A. S. Shandiz et al., "Novel imatinib-loaded silver nanoparticles for enhanced apoptosis of human breast cancer MCF-7 cells," *Artif. Cells Nanomed. Biotechnol.*, vol. 45, no. 6, pp. 1115–1124, 2017, doi: 10.1080/21691401.2016.1202257.

[23] H. Danafar, A. Sharafi, S. Kheiri, and H. K. Manjili, "Co-delivery of sulforaphane and curcumin with PEGylated iron oxide-gold core shell

nanoparticles for delivery to breast cancer cell line," *Int. J. Pharm. Res.*, vol. 10, no. 2, pp. 1–12, Apr. 2018.

[24] J. Li, J. Wang, and Z. Chen, "Emerging role of exosomes in cancer therapy: Progress and challenges," *Mol. Cancer*, vol. 23, p. 233, Dec. 2024, doi: 10.1186/s12943-024-02215-4.

[25] B. Wang et al., "Current advance of nanotechnology in diagnosis and treatment for malignant tumors," *Signal Transduct. Target. Ther.*, vol. 9, p. 218, Aug. 2024, doi: 10.1038/s41392-024-01889-y.

[26] L. M. Bareford and P. W. Swaan, "Endocytic mechanisms for targeted drug delivery," *Adv. Drug Deliv. Rev.*, vol. 59, no. 8, pp. 748–758, Aug. 2007, doi: 10.1016/j.addr.2007.06.010.

[27] K. J. Livak and T. D. Schmittgen, "Analysis of relative gene expression data using real-time quantitative PCR and the 2−ΔΔCt method," *Methods*, vol. 25, no. 4, pp. 402–408, Dec. 2001, doi: 10.1006/meth.2001.1262.

[28] S. A. Bustin et al., "The MIQE guidelines: Minimum information for publication of quantitative real-time PCR experiments," *Clin. Chem.*, vol. 55, no. 4, pp. 611–622, Apr. 2009, doi: 10.1373/clinchem.2008.112797.

[29] A. Sharmila et al., "Nanoformulated terpenoids in cancer: A review of therapeutic applications, mechanisms, and challenges," *Cancers*, vol. 17, no. 18, p. 3013, Sep. 2025, doi: 10.3390/cancers17183013.

[30] A. Sarkar, S. Ghosh, S. Chowdhury, B. Pandey, and P. C. Sil, "Targeted delivery of quercetin loaded mesoporous silica nanoparticles to the breast cancer cells," *Int. J. Pharm.*, vol. 503, no. 1–2, pp. 282–291, May 2016, doi: 10.1016/j.ijpharm.2016.05.024.

[31] S. A. S. Shandiz et al., "Novel imatinib-loaded silver nanoparticles for enhanced apoptosis of human breast cancer MCF-7 cells," *Artif. Cells Nanomed. Biotechnol.*, vol. 45, no. 6, pp. 1115–1124, 2017, doi: 10.1080/21691401.2016.1202257.

[32] V. Are et al., "Combination therapy of Lapatinib/Letrozole-based protein-vitamin nanoparticles to enhance the therapeutic effectiveness in drug-resistant

breast cancer," *Int. J. Pharm.*, vol. 770, p. 125899, Nov. 2024, doi: 10.1016/j.ijpharm.2024.125899.

[33] S. Chapman et al., "Nanoparticles for cancer imaging: The good, the bad, and the promise," *Wiley Interdiscip. Rev. Nanomed. Nanobiotechnol.*, vol. 5, no. 5, pp. 553–568, Sep./Oct. 2013, doi: 10.1002/wnan.1234.

[34] S. A. Bustin et al., "The MIQE guidelines: Minimum information for publication of quantitative real-time PCR experiments," *Clin. Chem.*, vol. 55, no. 4, pp. 611–622, Apr. 2009, doi: 10.1373/clinchem.2008.112797.

[35] A. Sharmila et al., "Nanoformulated terpenoids in cancer: A review of therapeutic applications, mechanisms, and challenges," *Cancers*, vol. 17, no. 18, p. 3013, Sep. 2025, doi: 10.3390/cancers17183013.

[36] B. Wang et al., "Current advance of nanotechnology in diagnosis and treatment for malignant tumors," *Signal Transduct. Target. Ther.*, vol. 9, p. 218, Aug. 2024, doi: 10.1038/s41392-024-01889-y.

[37] K. J. Livak and T. D. Schmittgen, "Analysis of relative gene expression data using real-time quantitative PCR and the 2−ΔΔCt method," *Methods*, vol. 25, no. 4, pp. 402–408, Dec. 2001, doi: 10.1006/meth.2001.1262.

[38] S. Imtiaz et al., "Mechanistic study of cancer drug delivery: Current techniques, limitations, and future prospects," *Eur. J. Med. Chem.*, vol. 293, p. 117350, May 2025, doi: 10.1016/j.ejmech.2025.117350.